Microstructure characterisation of $Al_{65}Cr_{28}Fe_7$ quasicrystalline approximant

J. Janovec[1]*, M. Svoboda[2], J. Dolinšek[3], M. Godec[4], J. Buršík[2], J. Dusza[5]

[1] *Slovak University of Technology, Faculty of Materials Science and Technology, Department of Materials Engineering, Bottova 23, 917 24 Trnava, Slovak Republic*
[2] *Academy of Sciences of the Czech Republic, Institute of Physics of Materials, Žižkova 22, 616 62 Brno, Czech Republic*
[3] *Jožef Stefan Institute, University of Ljubljana, Jamova 39, 1000 Ljubljana, Slovenia*
[4] *Institute of Metals and Technology, Lepi pot 11, 1000 Ljubljana, Slovenia*
[5] *Slovak Academy of Sciences, Institute of Materials Research, Watsonova 47, 043 53 Košice, Slovak Republic*

Received 13 February 2006, received in revised form 21 October 2006, accepted 29 October 2006

Abstract

The microstructure characterisation of the quasicrystalline approximant $Al_{65}Cr_{28}Fe_7$ was performed by transmission electron microscopy, electron diffraction, scanning electron microscopy, energy dispersive X-ray spectroscopy, and other methods. In the investigated sample, two phases were identified: the metallic matrix possessing hexagonal structure with lattice parameters $a = 1.2728$ nm and $c = 0.7942$ nm (isostructural with the gamma-brass) and Al_2O_3 in the form of inclusions. The microstructure of the approximant was found to be formed by grains (their interior consists of plain and lamellate areas) surrounded by heterogeneous areas rich on the Al_2O_3 inclusions. The lamellate areas were found to be formed by parallel bands. Every other band showed the same orientation. In the band boundaries, the dislocation networks were found. It was shown that two sets of dislocations oriented nearly perpendicular to each other form dislocation networks also inside the bands.

K e y w o r d s: quasicrystalline approximant, substructure, transmission electron microscopy

1. Introduction

Quasicrystals are solid materials exhibiting a new kind of a perfect long-range order involving symmetries incompatible with the translation periodicity of the crystalline lattice. The binary and ternary aluminium-base alloys containing d-transition metals (V, Cr, Mn, Fe, Co, Ni, Mo, Tc, Ru, Rh, Pd, W, Re, Os, Ir and Pt) were found to be suitable systems for formation of quasicrystalline phases [1–3]. It is generally known that the first quasicrystalline phase of the icosahedral symmetry was discovered in a rapidly solidified Al-Mn alloy, about twenty years ago [4]. The later structural and compositional studies showed that both stable and metastable quasicrystals can be formed in aluminium alloys when the bulk aluminium content ranges between 60–85 at.% [3]. In ternary alloys, the stable quasicrystals formed incongruently by reactions containing the liquid phase were identified mainly. They were found to persist during annealing for long times at temperatures just below solidus that gives evidence about their thermodynamic stability. The stable quasicrystals possess either the three-dimensional icosahedral (*I-type*) or the two-dimensional decagonal (*D-type*) structures [5, 6]. Some quasicrystalline phases formed at higher temperatures show tendency to the periodic rearrangements in submicrodomains [7, 8] or to the formation of definitely periodic structures if annealed at lower temperatures [9]. These phases are classified as metastable quasicrystals, and their low-temperature modifications are also named *quasicrystalline approximants*. In some binary systems, both the quasicrystalline and the crystalline phases of similar chemical compositions can be formed. The atomic order in the crystalline phase (named also neighbouring phase) shows tendency to the icosahedral symmetry, but it is constrained by periodicity [3, 10]. There are small dif-

*Corresponding author: tel.: +421 918646072; fax: +421 335521019; e-mail address: jozef.janovec@stuba.sk

ferences only between the formation enthalpies of the stable quasicrystals and the neighbouring crystalline phases [11].

Quasicrystals and quasicrystalline approximants can possess lamellate structures observable by transmission (TEM) and/or high resolution electron microscopy (HREM). For instance, Mukhopadhyay et al. [12, 13] found in the D-type $Al_{62}Cu_{20}Co_{15}Si_{13}$ phase rhombic domains containing fine parallel lines (referred to as striations). The striations appeared in all orientations perpendicular to the ⟨100000⟩ direction. The lowest spacing of the striations was found to be 0.5–0.6 nm. According to Mukhopadhyay et al. [12], the striations were formed due to the phason-type disordering in superordered structures. Phasons in quasicrystals represent static displacement fields (so-called phason strains) introducing static disorder into the perfect quasicrystalline structures [14–16]. Due to the phason appearance, some of the reflection spots are broadened in electron diffraction patterns. The striation contrasts observed in quasicrystalline phases by TEM were attributed either to small crystalline regions in quasiperiodic structures [17] or to twins present in microcrystalline phases [18, 19]. The latter type of the lamellate structures is referred to as tweed structure. In the f.c.c. matrix the tweed structure consists of parallel twinned bands possessing the ordered face-centred tetragonal structure [19, 20]. The width of individual bands ranges between 50 and 100 nm, microtwins lying within the bands (i.e. striations) are thick less than 10 nm. The disorientation angle between two neighbour bands is 120°, every other band has the same orientation. The above described tweed structures were observed in dental alloys 76Pd-10Cu-5.5Ga-6Sn-2Au and 75Pd-6Ga-6In-6Au-6.5Ag showing similar lattice arrangements as the quasicrystalline approximants [20].

The quasicrystalline approximants were found to exhibit intermediate physical properties related to regular crystals and stable quasicrystals. For instance, the values of electrical resistivity increase in sequence: regular crystals → quasicrystalline approximants → stable quasicrystals [21, 22]. Regarding the thermal conductivity at room temperature, the electronic contribution is dominant in regular crystals whereas the lattice contribution is dominant in stable quasicrystals. For quasicrystalline approximants, the electronic and lattice contributions were found to be of comparable sizes that ranks them in-between the regular crystals and the stable quasicrystals [21, 23]. At low temperatures (under 40 K) the heat transport can be limited, however, by scattering of phonons at internal surfaces. The interfaces in lamellate structures should be convenient places for phonon scattering. It is important therefore to know how the basic structural units are arranged, before the physical properties of quasicrystalline approximants are interpreted.

Characterisation of the quasicrystalline approximant $Al_{65}Cr_{28}Fe_7$ is the main aim of this work. The study was done with the intention to describe microstructure (substructure) of the approximant by various techniques and at different steps of exactness. We assessed therefore metallurgical purity, structural integrity, chemical homogeneity, and microstructure of the approximant. The attention was paid to the investigation of lamellate structures. In the next step the results of this work will be completed by measurements of electrical resistance, thermal conductivity and other physical properties.

2. Material and experiments

The $Al_{65}Cr_{28}Fe_7$ sample was prepared by melting the pure constituents under helium atmosphere in an induction furnace. The as-cast ingots were then crushed into powder of granulometric fractions between 20 and 50 μm. The powder was compactised in a graphite cell, sintered at 1060 ℃ using a uniaxial pressure of 15 MPa and annealed at 100 ℃ for 2 h.

The samples for metallographic observations were grinded, polished, and finally etched in 0.5% aqueous solution of fluoric acid. The light microscopy (LM) images were made using a NIKOM MICROPHOT FXA microscope equipped with a HITACHI HV-C20X videocasette camera.

Hardness of the sample was measured by means of semi-automatic tester SHIMATSU M using a Vickers indentor. Indentation was done at the load of 15 g with the pre-determined dwell time of 10 s. The instrument provided semi-automatic measurements of diagonals and automatic calculations of the HV 0.015 values.

Thin foils for the TEM observations were prepared by precision ion polishing in a GATAN 656 mill. Phases present in the $Al_{65}Cr_{28}Fe_7$ sample were identified by means of the selected area electron diffraction (SAD) and the energy dispersive X-ray spectroscopy (EDX). The TEM investigations were done in a Philips CM12 microscope operating at 120 kV.

Scanning electron microscopy (SEM) was used to observe etched surfaces of the metallographic sample and to determine distribution of chemical elements across the sample. The SEM investigations were performed by JEOL JSM 6500F microscope equipped with an EDS INCA ENERGY 400 analyzer enabling EDX analysis.

3. Results

Microstructure (LM) of the $Al_{65}Cr_{28}Fe_7$ sample is documented in Fig. 1. It consists of the plain, lamellate and heterogeneous areas named according to the characteristic microstructural features. Results of the

Table 1. Average values of hardness HV 0.015 for plain, lamellate, and heterogeneous areas

Area	Number of measurements	HV 0.015
Plain	13	868 ± 76
Lamellate	9	839 ± 81
Heterogeneous	19	902 ± 101
Total	41	877 ± 91

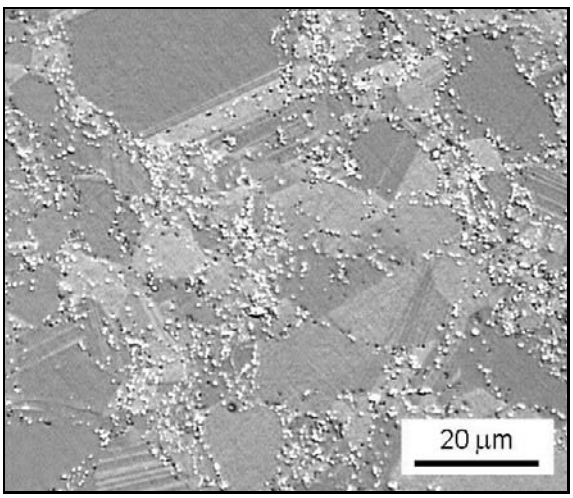

Fig. 1. Micrograph showing microstructure of the $Al_{65}Cr_{28}Fe_7$ approximant consisting of plain, lamellate and heterogeneous areas, LM. Etched in 0.5% water solution of fluoric acid.

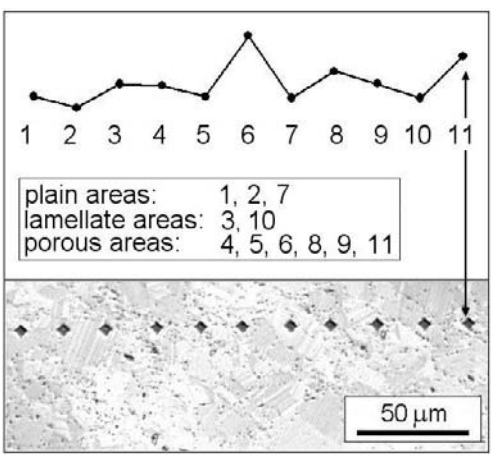

Fig. 2. Couples formed by the HV 0.015 value (upper part) and the corresponding indentation (lower part) for different areas of the $Al_{65}Cr_{28}Fe_7$ approximant, LM. Numbers 1 to 11 are used to mark the couples.

hardness measurements are shown in Fig. 2 and summarised in Table 1. In Fig. 2, dimensions of the in-

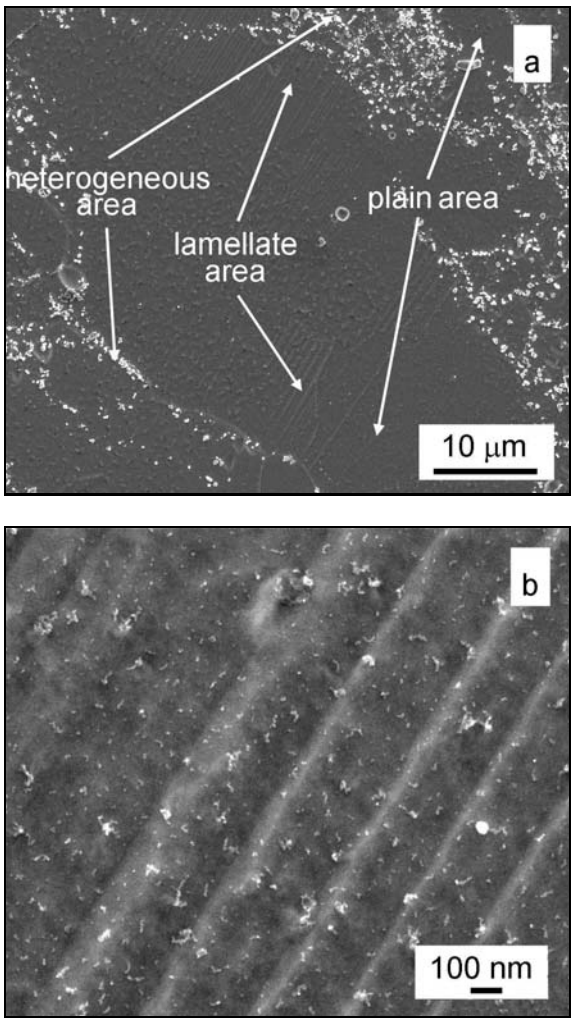

Fig. 3. Secondary electron images of etched surfaces of the $Al_{65}Cr_{28}Fe_7$ approximant, SEM: a) morphology of plain, lamellate and heterogeneous areas, b) details of the lamellate area.

dentations in the particular areas are related to the values of HV 0.015. There are small differences only between the values of hardness measured for various areas. However, the average hardness of the heterogeneous area is a bit higher than those of other two areas (Table 1). To obtain more detail images of the plain, lamellate and heterogeneous areas, the etched metallographic samples were also observed by scanning electron microscopy (Fig. 3). In the secondary electrons images the following microstructure features are noticeable:

– the protrusions present in the plain areas, giving similar contrasts as the surrounding matrix (Fig. 3a); they are probably etching artefacts,

– the white-colour objects of various sizes present in the heterogeneous areas (Fig. 3a); in the back-scattered electron image (compare Figs. 4a and 4b) they give different contrasts (white and black),

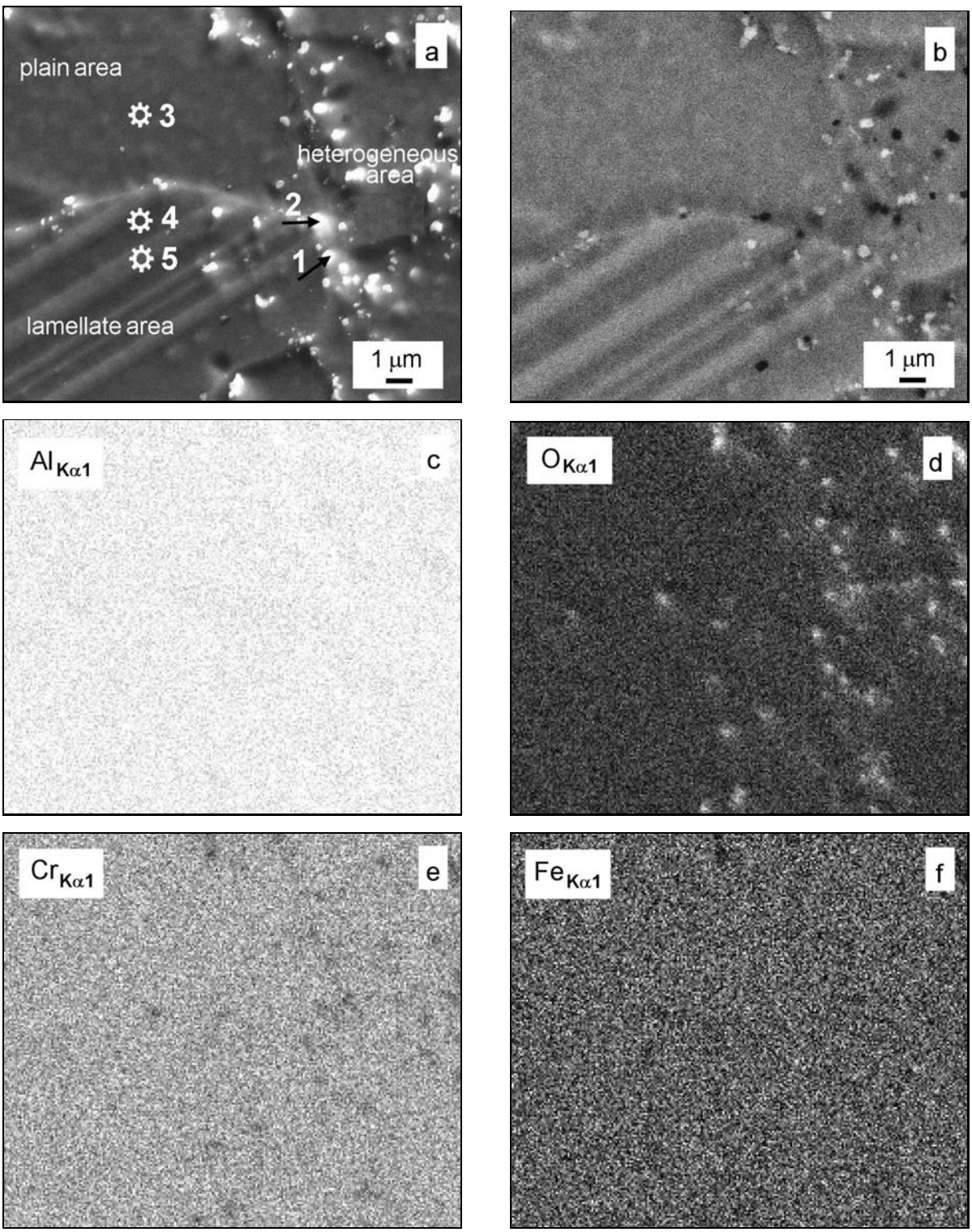

Fig. 4. Distribution of elements in plain, lamellate and heterogeneous areas of the $Al_{65}Cr_{28}Fe_7$ approximant, SEM: a) secondary electron image; b) back-scattered electron image of the same locality as documented under a); c) distribution of aluminium in locality documented under a), for mapping the peak $Al_{K\alpha1}$ was used, EDX; d) distribution of oxygen in locality documented under a), for mapping the peak $O_{K\alpha1}$ was used, EDX; e) distribution of chromium in locality documented under a), for mapping the peak $Cr_{K\alpha1}$ was used, EDX; f) distribution of iron in locality documented under a), for mapping the peak $Fe_{K\alpha1}$ was used, EDX.

– the lamellate areas consisting of parallel bands (Fig. 3b); white fibres on the sample surface are probably products of etching.

The results of EDX analyses and the maps showing

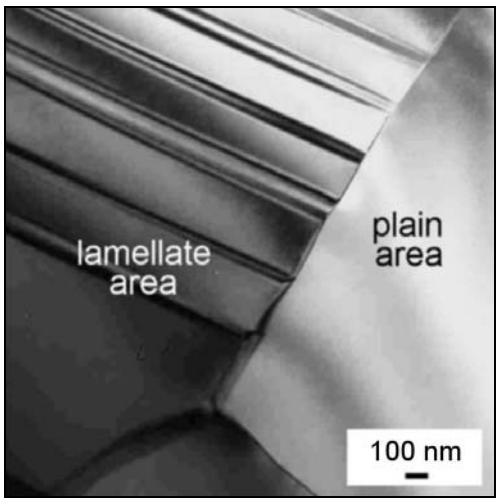

Fig. 5. Bright field image showing boundary between the lamellate and plain areas of the $Al_{65}Cr_{28}Fe_7$ approximant, TEM. Orientation of the thin foil was not determined.

distributions of aluminium, oxygen, chromium, and iron across the sample are illustrated in Fig. 4 and summarised in Table 2. The plain areas as well as bands present in the lamellate areas (marked with respective numbers 3, 4, and 5 in Fig. 4a) possess chemical compositions comparable with the stoichiometry of the approximant. Besides the basic metallic elements (aluminium, chromium, iron), oxygen was also identified in the plain and lamellate areas (Table 2). Aluminium and oxygen are dominant elements in the white-colour objects. This fact follows from both the data given in Table 2 and the maps illustrated in Figs. 4c–f. Except for the white-colour objects, distributions of all metallic elements across the sample are rather uniform (Figs. 4c–f).

In Fig. 5, boundaries between grains and bands within the lamellate area are documented. Crystal structure of the approximant was determined for the plain area (Fig. 6). The diffraction patterns taken for three different zone axes give evidence about the hexagonal (rhombohedral) structure with the lattice parameters: $a = 1.2728$ nm and $c = 0.7942$ nm. Thus, the approximant is isostructural with the gamma-brass, type Al_8Cr_5, space group *R3m* (No. 160) [24].

As is evident from Fig. 7, the substructure of the lamellate area is formed by parallel bands. The bands are thick several hundred nanometers, and every other band shows the same orientation. In the interior of the bands, two sets of dislocations oriented nearly perpendicular to each other form the dislocation network (Fig. 7a). Dislocations of the first set correspond to the bright lines, dislocation of the second set correspond to the grey fields crossing the lines. Details of the dislocation arrangement are illustrated in Fig. 7b. In Fig. 8, arrangement of dislocations in the band boundary is illustrated. It is evident from the figure that a dislocation network occurs in the boundary plane.

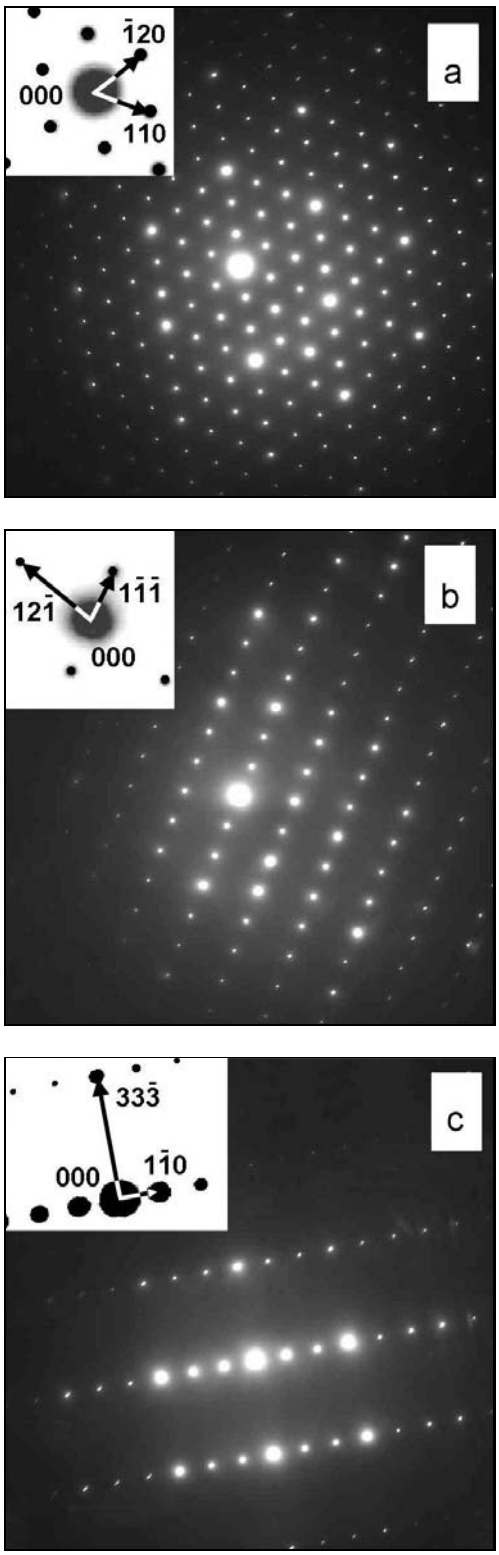

Fig. 6. Selected area diffraction patterns for the plain area of the $Al_{65}Cr_{28}Fe_7$ approximant in three different orientations, TEM: a) $\mathbf{B} = [001]$, b) $\mathbf{B} = [101]$, c) $\mathbf{B} = [112]$. The diffraction patterns are indexed in the left upper corner of the figures.

Table 2. Results of the local chemical analysis of the $Al_{65}Cr_{28}Fe_7$ approximant, EDX/SEM. The analysed places are marked with symbols 1 to 5 in Fig. 4a

Analysed place	Area	Object	Atomic content of element in %			
			Al	O	Cr	Fe
1	heterogeneous	particle	44	40	13	3
2	heterogeneous	particle	48	31	17	4
3	plain	bulk	62	3	28	7
4	lamellate	bulk	61	3	29	7
5	lamellate	bulk	62	3	28	7

Particle of Al_2O_3 present in the heterogeneous area of the $Al_{65}Cr_{28}Fe_7$ sample is documented in Fig. 9. It is long about 600 nm, and shows sharp edges. Any other types of particles were not identified in the substructure of the sample.

4. Discussion

The experimental measurements performed in this work uncovered some original findings regarding the structure and properties (e.g. metallurgical purity, structural integrity, hardness, chemical homogeneity) of the $Al_{65}Cr_{28}Fe_7$ sample. They will be discussed in the next paragraphs in more detail.

4.1. Microstructural characterisation of the approximant

Two phases were identified in the microstructure of the sample: the matrix of the hexagonal structure and Al_2O_3 inclusions (Table 2, Fig. 9). The inclusions originate probably from the aluminium powder. Sharp edges of the inclusions show their morphological stability during sintering and/or annealing (Fig. 9). The inclusions are cumulated in the heterogeneous areas separating from each other grains formed by the plain and lamellate areas. The heterogeneous areas were formed probably from surfaces of the original aluminium granules during sintering. Then, the plain and lamellate areas should correspond to the internal parts of the granules. Widths of the heterogeneous areas range between 1 and 30 μm (Figs. 1, 3a, 4a). Isolated inclusions were also observed outside the heterogeneous area (Figs. 3a, 4a). They are responsible probably for the presence of oxygen (3 at.%) in the plane and/or lamellate areas (Table 2).

Small black objects observed in the microstructure of the sample (Fig. 1) can be either voids after fell out particles or pores. To solve this problem a contrast SEM image was prepared in back-scattered electrons (Fig. 4b) parallel to that in secondary electrons (Fig. 4a). The image shows that the dimensions of voids and particles are comparable. It favours the first of the above possibilities (voids after fell out particles). In other words, the procedures used in processing of the sample do not leave any observable porosity in the material.

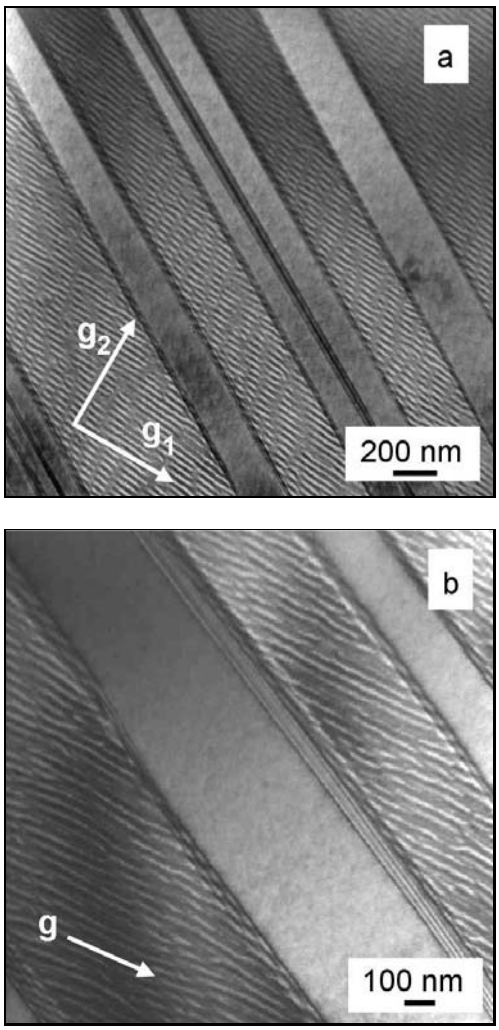

Fig. 7. Bright field images in double-beam condition showing arrangement of dislocations in the lamellate area of the $Al_{65}Cr_{28}Fe_7$ approximant, TEM: a) two sets of dislocations oriented nearly perpendicular to each other ($\boldsymbol{g}_1 \perp \boldsymbol{g}_2$), $\mathbf{B} = [001]$, $\boldsymbol{g}_1 = 110$, $\boldsymbol{g}_2 = \bar{1}10$, b) details, $\mathbf{B} = [001]$, $\boldsymbol{g} = 110$.

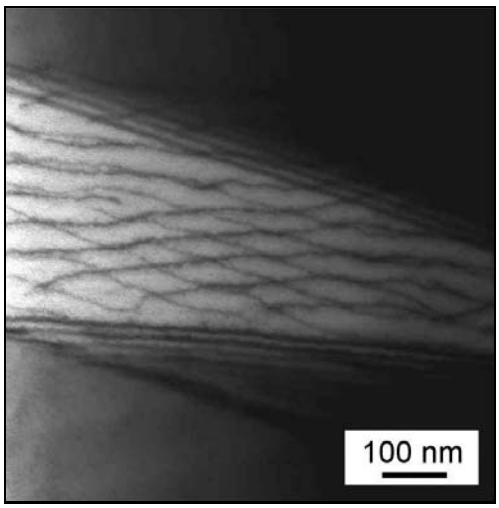

Fig. 8. Bright field image of the dislocation network in boundary between two bands of the lamellate area, TEM. Both sets of dislocations show the same contrast. Orientation of thin foil was not determined.

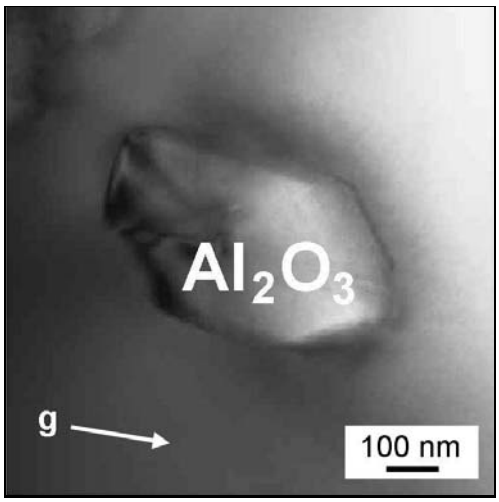

Fig. 9. Bright field image of Al_2O_3 particle in heterogeneous area of the $Al_{65}Cr_{28}Fe_7$ approximant, TEM. $\mathbf{B} = [100]$, $\boldsymbol{g} = 01\bar{1}$.

Both the identified phases (see above) are of crystalline nature. There were not found any quasicrystalline and/or amorphous objects in the microstructure. The matrix phase formed by the quasicrystalline approximant was found to be homogeneous from the chemical point of view (Table 2, Figs. 4c–f). From the structural viewpoint the matrix phase can be considered as an approximant of both icosahedral and decagonal quasicrystals [25]. Even if a part of the matrix phase consists of lamellate areas, this fact does not show any significant influence on hardness of the microstructure (Fig. 2). It was found out that the lamellate areas are located within the grains separated from each other by heterogeneous areas, and bands forming the lamellate areas cannot cross the grain boundaries (Figs. 1, 4a, 4b, 5). A possible mechanism of the formation of the lamellate areas is described in the next paragraph.

4.2. Characterisation of lamellate structures

The investigations done in this work led to the following findings concerning the bands present in the lamellate areas:

– the approximant proves the same crystal structure within the bands and in the surrounding matrix,

– every other band shows the same orientation that gives evidence about different orientation of two neighbour bands (Fig. 7),

– thickness of the band proves hundreds of nanometers,

– the band boundaries are oriented parallel to each other and contain dislocation networks (Fig. 8),

– two sets of dislocations oriented nearly perpendicular to each other form the dislocation network in the interior of the bands (Fig. 7a).

The lamellate structure characterised in this work is similar to the tweed bands identified by Guo et al. [20] in the dental alloys 76Pd-10Cu-5.5Ga-6Sn-2Au and 75Pd-6Ga-6In-6Au-6.5Ag. The differences concern thickness and the band fine structure only. The bands described in this work are wider than those described by Guo et al. [20] and their interiors contain dislocation network instead of microtwins observed in tweed bands. The tweed bands were formed during the plastic deformation due to the effort to compensate the external strain. It is highly probable that the bands described in this work were also formed as a consequence of the local deformation during processing of the sample. One can suppose that the internal stresses across the processed material were not distributed uniformly. The best conditions for the band formation were in localities with the highest stresses. This suggestion supports also the fact that the lamellate area does not fill all volume of the grain, but its part only.

It is generally known that the transport phenomena as electrical, optical and thermal conductivity, diffusion etc. are strongly structurally dependent [22, 26]. The pure material with the near ideal arrangement of atoms is an optimal object for study of transport phenomena. From this point of view, three important imperfections were found in the microstructure of the sample formed prevailingly by the quasicrystalline approximant:

– the Al_2O_3 inclusions themselves represent isolators forming the incoherent interfaces with the surrounding metallic matrix,

– the heterogeneous areas rich on the Al_2O_3 inclusions,

– the band boundaries and the dislocation networks in the lamellate areas.

All these factors should contribute to deterioration of the transport properties compared to the ideal state. Otherwise, the plain areas of the approximant possess satisfactory chemical and structural homogeneity.

5. Conclusions

The microstructure characterisation of the investigated sample revealed the following findings:

1. Two phases were identified in the sample. The first one is the metallic matrix possessing hexagonal structure with lattice parameters: $a = 1.2728$ nm and $c = 0.7942$ nm. It is isostructural with the gamma-brass (type Al_8Cr_5, space group No. 160). The matrix phase showed chemical homogeneity and was classified as a quasicrystalline approximant. The second phase is Al_2O_3 in the form of inclusions.

2. The microstructure of the sample is formed by grains surrounded by heterogeneous areas rich of the Al_2O_3 inclusions. The interior of the grains consists of plain and lamellate areas.

3. There were not identified any quasicrystalline or amorphous objects in the analysed material. Procedures used in processing of the approximant do not leave any observable porosity.

4. The lamellate areas are formed by parallel bands, which do not cross the grain boundaries. The band thickness proves hundreds of nanometers. Every other band shows the same orientation. In the band boundaries, dislocation networks were found.

5. It was shown that two sets of dislocations oriented nearly perpendicular to each other form dislocation networks inside the bands.

6. The Al_2O_3 inclusions, the heterogeneous areas rich of the Al_2O_3 inclusions, and the lamellate areas containing dislocation networks were considered to be factors contributing to the deterioration of transport properties of the approximant.

Acknowledgements

The authors of this work cooperated in the framework of the 6th FP NoE *Complex Metallic Alloys*. They wish to thank Nataša Lipovšek and Irena Kranjc of the Institute of Metals and Technology in Ljubljana for the assistance in metallographic observations and microhardness measurements as well as Miroslav Daniel of the Institute of Physics of Materials AS CR in Brno for the preparation of TEM samples.

References

[1] JANOT, C.—DUBOIS, J. M.: J. Phys. F, *18*, 1988, p. 2303.

[2] SHECK, C. H.—HE, G.—BIAN, Z.—CHEN, G. L.—LAI, J. K. L.: Mater. Sci. Engn., *A357*, 2003, p. 20.

[3] GRUSHKO, B.—VELIKANOVA, T. Z.: J. Alloys Compd., *367*, 2004, p. 58.

[4] SHECHTMAN, D.—BLECH, I.—GRATIAS, J.—CAHN, J.: Phys. Rev. Lett., *53*, 1984, p. 1951.

[5] STEURER, W.—KUO, K. H.: Acta Crystallogr., *B46*, 1990, p. 703.

[6] STEURER, W.—HAILBAH, T.—ZHANG, B.—KEK, S.—LUCK, R: Acta Crystallogr., *B49*, 1993, p. 661.

[7] FETTWEIS, M.—LAUNOIS, P.—REICH, R.—WITTMANN, R.—DÉNOYER, F.: Phys. Rev. B, *51*, 1995, p. 6700.

[8] DÖBLINGER, M.—WITTMANN, R.—GRUSHKO, B.: Phys. Rev. B, *64*, 2001, p. 134208.

[9] QUIQUANDON, M.—QUIVY, A.—DEVAUD, J.—FAUDOT, F.—LFEBVRE, M.—BESSIERE, M.—CAVAYRAC, Y.: J. Phys. Condens. Matter, *8*, 1996, p. 2487.

[10] WIDOM, M.—PHILLIPS, R.—ZOU, J.—CARLSSON, A. E.: Phil. Mag. B, *71*, 1995, p. 397.

[11] SAÂDI, N.—HARMELIN, M.—FAUDOT, F.—LEGENDRE, B.: J. Non-Cryst. Solids, *153–154*, 1993, p. 500.

[12] MUKHOPADHYAY, N. K.—WEATHERLY, G. C.—SASTRY, G. V. S.: Mater. Sci. Engn., *294–296*, 2000, p. 135.

[13] MUKHOPADHYAY, N. K.—SASTRY, G. V. S.—WEATHERLY, G. C: Phil. Mag. A, *80*, 2000, p. 1795.

[14] DOLINŠEK, J.—APIH, T.—SIMSIČ, M.—DUBOIS, J. M.: Phys. Rev. Lett., *82*, 1999, p. 572.

[15] DOLINŠEK, J.—APIH, T.—JEGLIČ, P.—FEUERBACHER, M.—CALVO-DHLBORG, M.—DAHLBORG, U.—DUBOIS, J. M.: Phys. Rev. B, *65*, 2002, p. 212203.

[16] LUBENSKY, T. C.—RAMASWAMY, S.—TONER, J.: Phys. Rev. B, *32*, 1985, p. 7444.

[17] ZHANG, Z.—GENG, W.—VAN LANDUYT, J.—VAN TENDELOO, G.: Phil. Mag. A *71*, 1995, p. 1177.

[18] SONG, S.—WANG, L.—RYBA, E. R.: Phil. Mag. Lett., *63* , 1991, p. 355.

[19] CAI, Z.—BRANTLEY, W. A.—CLARK, W. A. T.—COLIJN, H. O.: Dent. Mater., *13*, 1997, p. 365.

[20] GUO, W. H.—BRANTLEY, W. A.—CLARK, W. A. T.—XIAO, J. Z. —PAPAZOGLOU, E.: Dent. Mater., *19*, 2003, p. 334.

[21] BIHAR, Ž.—BILUŠIĆ, A.—LUKATELA, J.—SMONTRA, A.—JEGLIČ, P.—McGUINESS, P. J.—DOLINŠEK, J.—JAGLIČIĆ, Z.—JANOVEC, J.—DEMANGE, V.—DUBOIS, J. M.: J. Alloys Comp., *407*, 2006, p. 65.

[22] DOLINŠEK, J.—KLANJŠEK, M.—JAGLIČIĆ, Z.—BILUŠIĆ, A.—SMONTRA, A.: J. Phys.: Condens. Matter, *14*, 2002, p. 6972.

[23] KRISCH, M.—BRAND, R. A.—CHEMIKOV, M. A.—OTT, H. R.: Phys. Rev. B, *65*, 2002, p. 134201.

[24] BRANDON, J. K.—PEARSON, W. B.—RILEY, P. W.—CHIEH, C.—STOCKHUYZEN, R.: Acta Crystallogr., *B33*, 1977, p. 1088.

[25] DONG, C.: Phil. Mag. A, *73*, 1996, p. 1519.

[26] DEMANGE, V.—MILANDRI, A.—DeWEERD, M. C.—MACHIZAUD, F.—JEANDEL, G.—DUBOIS, J. M.: Phys. Rev. B, *65*, 2002, p. 144205.